Relation between mesospheric ice clouds, temperature, and water vapor determined from Odin/OSIRIS and TIMED/SABER data

A. G. Feofilov[1,2] and S. V. Petelina[3]

Received 30 November 2009; revised 19 May 2010; accepted 27 May 2010; published 22 September 2010.

[1] Altitude, brightness, and occurrence rate of polar mesospheric clouds (PMCs) with respect to kinetic temperature, pressure, and water vapor volume mixing ratio (VMR) in the ice formation area are studied. Cloud and atmospheric parameters are measured by the Optical Spectrograph and Infrared Imager System and by the Sounding of the Atmosphere using Broadband Emission Radiometry satellite instruments, correspondingly. The analysis has been done for all northern and southern PMC seasons of 2002–2008 for both zonal averages and nearly simultaneous common volume measurements performed by two instruments. It has been found that PMC peak altitudes correlate well with mesopause altitudes, although the former experience lower seasonal variability. Mesopause temperatures anticorrelate with PMC occurrence rates and, in the Northern Hemisphere, show larger seasonal variability at high latitudes poleward of 75°N compared to 55°N–65°N. OSIRIS PMC brightness correlates with the vertical extent of the frost area and water vapor VMR below PMC (hydration effect) and anticorrelates with the mesopause temperature and water vapor VMR in the frost area (freeze-drying effect).

Citation: Feofilov, A. G., and S. V. Petelina (2010), Relation between mesospheric ice clouds, temperature, and water vapor determined from Odin/OSIRIS and TIMED/SABER data, *J. Geophys. Res.*, *115*, D18305, doi:10.1029/2009JD013619.

1. Introduction

[2] Ice particles, biggest of which constitute optically detectable polar mesospheric clouds (PMCs), form in the polar and midlatitude upper mesosphere during local summer when low temperatures permit ice nucleation and growth [e.g., *Thomas*, 1991; *Lübken*, 1999]. Such particles, composed of crystalline water ice [*Hervig et al.*, 2001; *Eremenko et al.*, 2005], nucleate at about 85–92 km, grow from a few nanometers to 70–90 nm radii, sediment to 81–83 km altitudes where temperatures become larger than the frost point temperature, evaporate, and produce the seasonal enhanced water vapor layer at altitudes around 80 km [e.g., *Rapp and Thomas*, 2006; *Hervig et al.*, 2009; *Robert et al.*, 2009, and references therein]. It is well known that the ice nucleation, growth, and evaporation processes, which determine the observed PMC properties, are greatly influenced by the surrounding temperature and water vapor and, to a lesser extent, by other parameters such as vertical winds, meteoric influx, and eddy diffusion [e.g., *Lübken et al.*, 2007]. Because of this, it is generally believed that the observed trends and changes in PMC properties can be used as a sensitive indicator of climate variability and climate change [e.g., *Thomas*, 2003; *Kirkwood et al.*, 2008; *Shettle et al.*, 2009]. Thus, understanding how the parameters of the surrounding environment affect PMC properties is important.

[3] Much more is known today about PMC ice particles compared to a decade ago. Measurements and models provide insights on possible mesospheric ice nucleation mechanisms, from a classical heterogeneous scenario [*Witt*, 1969; *Rapp and Thomas*, 2006, and references therein] to a recently proposed homogeneous scenario [*Zasetsky et al.*, 2009a; *Murray and Jensen*, 2009]. Ice growth times and equilibrium sizes have also been addressed with models and satellite and ground-based measurements [e.g., *Zasetsky et al.*, 2009b, and references therein]. The recently launched Aeronomy of Ice in the Mesosphere (AIM) satellite has been designed for further advancing these studies by simultaneously observing PMCs, temperature, water vapor, and meteoric dust.

[4] In this work, we study the qualitative and quantitative relation between PMC properties, namely peak altitude, occurrence frequency and brightness, and corresponding temperature and water vapor volume mixing ratio (H_2O VMR) using the coincident observations performed by two satellites in 2002–2008 in both hemispheres. The instruments used are: the Sounding of the Atmosphere using Broadband Emission Radiometry (SABER) instrument on the Thermosphere Ionosphere Mesosphere Energetics and Dynamics (TIMED) satellite and the Optical Spectrograph and Infrared Imager System (OSIRIS) on the Odin satellite.

2. Instrument and Data Description

2.1. TIMED/SABER

[5] The TIMED satellite was launched in December 2001 into a 74.1° inclination 625 km orbit with a period of 1.7 h.

[1]The Catholic University of America, Washington, D. C., USA.
[2]NASA Goddard Space Flight Center, Greenbelt, Maryland, USA.
[3]La Trobe University, Melbourne, Victoria, Australia.

0148-0227/10/2009JD013619

The TIMED mission is focused on the energetics and dynamics of the mesosphere–lower thermosphere region [*Yee et al.*, 1999]. SABER, one of four instruments on TIMED, is a 10-channel broadband limb-scanning infrared radiometer covering the spectral range from 1.27 to 17 μm. Among many other parameters, SABER provides vertical profiles of kinetic temperature, pressure, and water vapor. Its vertical instantaneous field of view is approximately 2.0 km at 60 km altitude, the vertical scanning step is ~0.4 km, and the atmosphere is scanned from below the surface up to 400 km tangent height. The instrument performs one vertical scan every 53 s. The latitudinal coverage has a 60 day yaw cycle that allows observing latitudes from 83°S to 52°N in the south viewing phase and from 53°S to 82°N in the north viewing phase. The instrument has been performing near-continuous measurements in this mode since 25 January 2002.

2.1.1. SABER Temperature Retrievals, Version 1.07

[6] The comprehensive analysis of the current SABER V1.07 temperatures is given by *Remsberg et al.* [2008]. Only features important for this work are highlighted below. SABER temperatures are retrieved from the limb radiance in the 15 μm CO_2 band that is formed by radiative transitions from the vibrationally rotationally excited levels of CO_2 molecules when the number of bending mode quanta (ν_2) changes by 1. Thus, a temperature retrieval algorithm needs a proper model for calculating the ν_2 levels populations. It is well known that these levels are in local thermodynamic equilibrium (LTE) with the media in troposphere and stratosphere, but in the mesosphere and above they depend on multiple local and nonlocal population and depopulation processes [*López-Puertas and Taylor*, 2001]. Among those, the ν_2 vibrational-vibrational (V−V) quanta exchanges between the CO_2 isotopes play an important role [*Kutepov et al.*, 2006]. The proper accounting for isotopic V−V exchanges in the non-LTE retrieval model has made SABER polar summer mesospheric temperatures (V1.07) more consistent with climatology [*Lübken*, 1999] and with individual rocket and ground-based measurements [*Goldberg et al.*, 2004; *Remsberg et al.*, 2008]. Since the deviation from the falling spheres climatology in the polar summer is larger for the twilight and nighttime retrievals compared to the daytime retrievals [see *Remsberg et al.*, 2008, Figures 24 and 25], only the daytime profiles were used in this work. For these retrievals, the mesopause altitude is ~1.5 km lower than that of the climatology and its temperature agrees well, within the retrieval accuracy, with that of the climatology. The estimated uncertainties for a single polar summer temperature profile are 2.0 K at 60 km, 1.6 K at 70km, 5.3 K at 80 km, and 10.4 K at 90 km [*Remsberg et al.*, 2008].

2.1.2. SABER Water Vapor Retrievals

[7] The water vapor volume mixing ratios (VMRs) are retrieved from the SABER limb radiances in the 6.3−7.3 μm spectral region. The populations of vibrational-rotational levels of the H_2O molecule responsible for the formation of these radiances are in non-LTE above ~60−65 km [*López-Puertas et al.*, 1995; *Manuilova et al.*, 2001]. It has been shown [*Zaragoza et al.*, 1998; *Edwards et al.*, 2000; *Manuilova et al.*, 2001; *Feofilov et al.*, 2009] that the solution of this system in the non-LTE area is sensitive to a number of reaction rates that are known with an insufficient accuracy. In this work, we use the set of rates for the H_2O non-LTE model estimated by *Feofilov et al.* [2009] from comparisons of SABER H_2O retrievals with coincident ACE-FTS H_2O profiles measured via solar occultation [*Bernath et al.*, 2005]. The SABER H_2O VMR retrievals were performed by ALI-ARMS research non-LTE code [*Kutepov et al.*, 1998; *Gusev and Kutepov*, 2003, and references therein] that solves the multilevel problem using the Accelerated Lambda Iteration technique [*Rybicki and Hummer*, 1991]. The retrieval algorithm utilizes a forward fitting approach where the process starts with an initial guess water vapor profile combined with a fixed atmospheric model (pressure, temperature, and VMRs of atmospheric gases retrieved from corresponding SABER measurements), solves the non-LTE problem, compares the simulated and measured radiances, and introduces the correction to H_2O VMR. The iterations are repeated until the differences between the simulated and measured radiances become equal to the radiance noise in the channel. The total uncertainty of a single SABER H_2O VMR profile retrieval estimated by *Feofilov et al.* [2009] is about 10% at and below 70 km, 20% at 80 km, and 30% at 85 km altitude.

2.2. Odin/OSIRIS

[8] Odin is an ongoing satellite mission launched in 2001 [*Murtagh et al.*, 2002] and devoted to aeronomy and, until the end of April 2007, astronomy studies. Odin is in a polar Sun-synchronous near-terminator orbit with the period of 96 min and the maximum latitudinal coverage in the orbit plane from 82.2°N to 82.2°S. OSIRIS measures the limb-scattered sunlight over the 280–810 nm range with ~1 nm spectral resolution and 0.2 km pointing precision. Its field of view is 1 km vertically and 32 km horizontally at the tangent point [*Llewellyn et al.*, 2004]. The OSIRIS exposure time in the mesosphere was set to 1.5–2 s in 2002–2003 and to 1 s in later years. Odin scans at the atmospheric limb with a speed of 0.75 km/s at the tangent point, and the OSIRIS vertical field of view varies between 1.3 and 2.3 km depending on the exposure time.

2.2.1. OSIRIS PMC Detections

[9] PMC detection from the OSIRIS limb measurements is based on the analysis of radiance enhancements at PMC altitudes, between 80 and 92 km, observed at each of several wavelengths in the UV region, namely 290.1, 294.0, 295.2, and 300.2 nm. This spectral region eliminates the effects of radiation upwelling from the troposphere and from the ground. A cloud is detected when the limb radiance exhibits an enhancement at one or more altitudes within the chosen range. Such enhancement must be present at each of the selected wavelengths. The ratio of the enhanced radiances at the chosen wavelengths is monitored as well. Further details on the OSIRIS PMC detection procedure can be found in the work of *Petelina et al.* [2006a, 2007].

2.2.2. PMC Altitudes

[10] Because of the nature of OSIRIS observations, the exact position of PMC peak within the instrument field of view is not known. We minimize this uncertainty by assigning the tangent altitude of a cloud peak to the center of the field of view. Such allocation, together with the 0.2 km pointing precision, yields a total random altitude error of up to 1.3 km for the minimal exposure time of 1 s [*Petelina et al.*, 2006b].

[11] The limb geometry of OSIRIS causes the detection of clouds located not only at the tangent point, but also in the near and/or far field of view. In the latter case, the clouds appear at lower altitudes. As it is not possible to distinguish between the clouds at the tangent point and those in the near/far field of view, certain restriction on PMC peak altitudes is necessary. Such restriction may vary depending on a particular task and, for this work, will be described later.

2.2.3. PMC Brightness

[12] The determination of PMC brightness from OSIRIS limb radiances is described in detail in [*Petelina et al.*, 2007]. Briefly, it is calculated as the difference between the measured limb radiance at PMC peak and the corresponding Rayleigh background. The Rayleigh background is assumed to be longitude independent and is derived from the statistically representative set of cloud-free limb profiles for each 1 km step in altitude and 1° step in latitude. To ensure high quality of data, the radiation enhancement caused by a PMC presence must be at least 3 times larger than the maximum uncertainty in the corresponding Rayleigh background. This uncertainty is caused primarily by the latitudinal changes in the solar scattering angle (SSA) and, to a lesser extent, by instrument noise and natural variations in atmospheric density. The maximum absolute value for the Rayleigh background uncertainty at 83 km does not exceed 1.5×10^9 photons/(nm·cm^2·s·sterad) at 290.1 nm. The average instrument noise at 290.1 nm is about 5 times smaller than the Rayleigh background uncertainty at 83 km.

[13] Similar to the Rayleigh background, PMC brightness is also dependent on the SSA, which varies from 87° to 95° in the morning sector and from 80° to 87° in the evening sector of the orbit. In this work, we have omitted any correction of brightness to the SSA as this would require the PMC scattering phase function for each individual cloud. As described in the work of *Petelina et al.* [2006b], using the phase function measured by *Gumbel et al.* [2001] yields a systematic error in PMC brightness of up to 30% at the lowest latitudes near 55°, but much smaller error near the polar regions.

2.3. Local Times for OSIRIS and SABER

[14] Odin crosses the equator at 18:00 local time (LT) on the ascending node and at 06:00 LT on the descending node. It goes through a range of LT very quickly poleward of 80°N, but very slowly at 50°N–70°N. At 60°N, for example, clouds are detected near 0700 LT on the downleg and near 1730 LT on the upleg of the orbit. Measurements at the highest latitude, 82.2°N, are taken near 1200 LT. PMC observations from all LT between 0700 and 1730 are used in this work. The OSIRIS observation geometry ensures equal probability of PMC detections in the morning and evening sectors. However, the number of morning and evening PMC detections may be different due to local time effects [e.g., *Fiedler et al.*, 2005; *Stevens et al.*, 2009].

[15] Different from OSIRIS, SABER samples the atmospheric parameters with LT variation within a yaw period. The measurement for each given latitude is made twice: on an ascending and descending mode with 12 h difference in LT. The precession of the TIMED orbit in respect with LT has a 60 days period. Because of the properties of the orbit measurements between 1100 and 1300 LT are not possible. While the discrepancy between OSIRIS and SABER LT coverage may influence the climatological analysis in section 3.2, coincident observations described in section 3.3 are not affected by the diurnal variability in mesospheric properties.

3. Results and Discussion

3.1. Climatological and "Instantaneous Snapshot" Approaches

[16] Two approaches to study the relation between PMC properties and pressure, temperature, and water vapor in the mesosphere are utilized. In the "climatological" approach, the weekly averages of these parameters are analyzed and the links between PMC altitudes and occurrence rates, average temperatures at PMC peak altitudes, and average mesopause temperatures are examined. An obvious reverse side of better statistics obtained for zonal averages is washing out of all local effects and mixing together the events that happened in different place and in different time. This problem is avoided in the "instantaneous snapshot" approach where we search the OSIRIS and SABER databases for nearly simultaneous common volume measurements using strict overlapping criteria. For these overlapping scans the OSIRIS PMC brightness is analyzed with respect to a vertical extent of the area where clouds are allowed to form (where the temperature is below the frost point). The latter is calculated using the coincident SABER measurements. The observed PMC brightness is also compared to the water vapor VMR in and below the cloud and to the mesopause temperature. The "instantaneous snapshot" approach does not take into account the PMC dynamics due to a lack of information on mesospheric winds. This adds a nonlocal component to the correlations we study. The particle growth dynamics also affects these correlations. However, as will be shown in section 3.3.3, the PMC properties are, to some extent, related to its local environment.

3.2. PMC-Temperature Relation for Zonal Averages

[17] SABER temperature profiles are used to determine the mesopause altitudes H_{mesop} and corresponding mesopause temperatures T_{mesop} during northern and southern PMC seasons in 2002–2008. These values are zonally averaged in the following six latitude belts: 55°N/S–65°N/S, 65°N/S–75°N/S, and 75°N/S–85°N/S, and the 7 day sliding window smoothing procedure is applied. The OSIRIS PMC data are processed in a similar way: with a 7 day sliding averaging for zonal mean cloud peak altitudes H_{PMC} and occurrence rates. In this work, PMC detections are restricted to clouds with peak altitudes at and above 80 km. The resulting relations between zonal mean H_{PMC} and zonal mean H_{mesop} are shown in Figure 1.

[18] SABER observes the summer polar latitudes only until day 25 from solstice in each hemisphere (except for the southern season of 2007–2008 when the observations stopped earlier), and this sets the last day for the analysis. First PMCs appear at various times depending on the solar cycle, atmospheric dynamics, and other factors [e.g., *Bailey et al.*, 2005; *DeLand et al.*, 2006], and the earliest OSIRIS observation of a PMC, day -30 from solstice, is selected as the first day for this analysis. As follows from Figure 1,

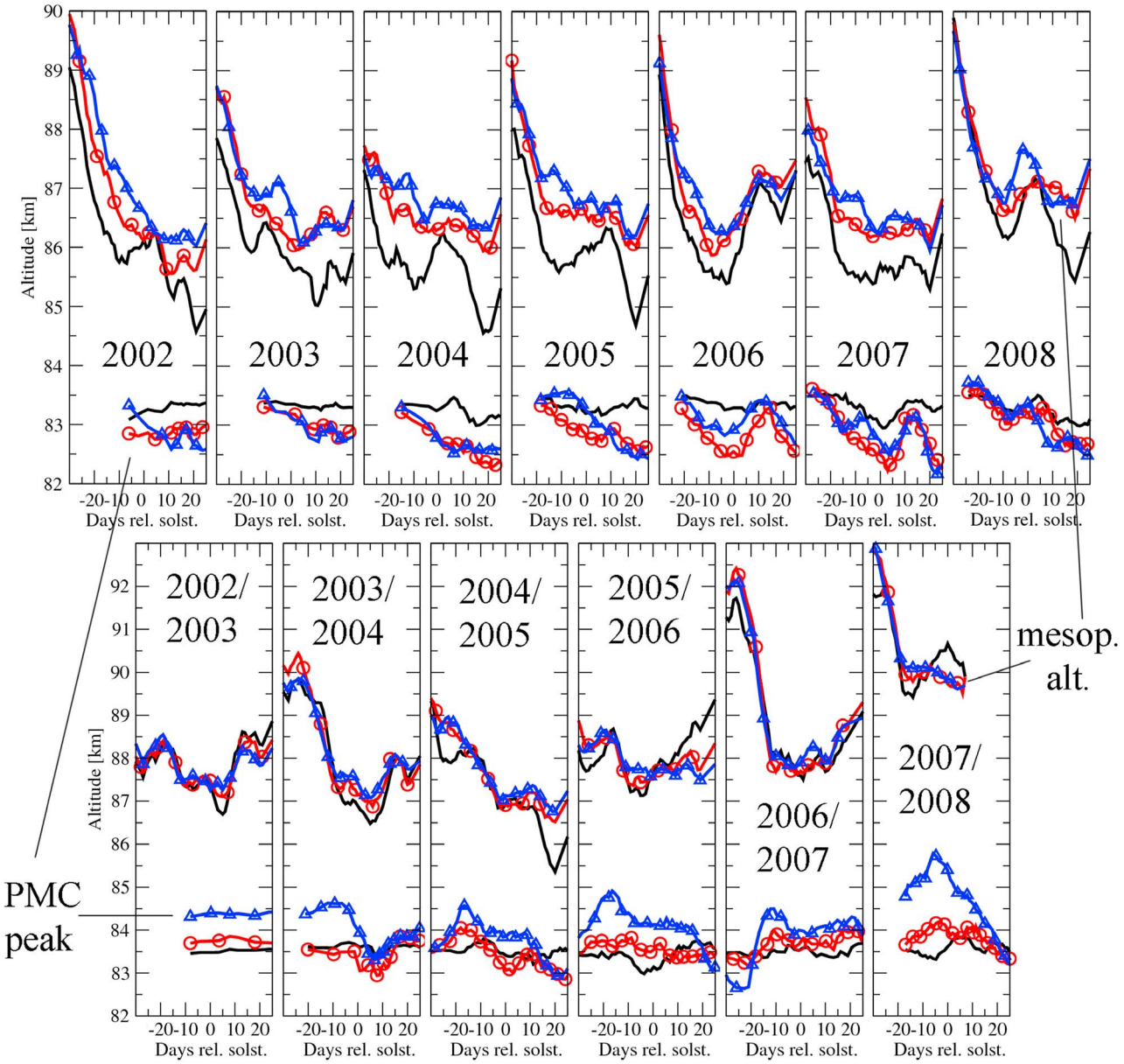

Figure 1. Zonal mean mesopause altitudes measured by SABER (top three curves in each frame) and zonal mean PMC peak altitudes measured by OSIRIS (three bottom curves in each frame) in the (top) NH and (bottom) SH. Solid curves: latitudes 55°N/S–65°N/S; curves with circles: latitudes 65°N/S–75°N/S; curves with triangles: latitudes 75°N/S–85°N/S.

H_{mesop} in the Northern Hemisphere (NH) is ~1.5 km lower than that in the Southern Hemisphere (SH). While the NH H_{mesop} experiences considerable latitudinal variability, much less variability is seen in the SH H_{mesop}. The average PMC peak altitude H_{PMC} is about 0.7 km higher in the SH compared to the NH.

[19] Variations in H_{mesop} and H_{PMC} appear to be correlated. Table 1 shows the maximized (as explained below) linear correlation coefficients K_{corr} for H_{mesop} and H_{PMC} calculated separately for each latitudinal belt in both hemispheres in 2002–2008. Each column of K_{corr} values in Table 1 is accompanied with the "Lag" value: the time lag between H_{mesop} and H_{PMC} that maximizes K_{corr}. If K_{corr} was lower than 0.3 and it changed its sign multiple times within ±7 days lag variation, then neither K_{corr} nor time lag values were assigned. As follows from Table 1, H_{mesop} and H_{PMC} are better correlated in the NH where $K_{corr} > 0.5$ for more than half of the cases. Their anticorrelation for latitudes near 60°N in 2002 is related to anomalously high mesospheric temperatures at that time. A zero time lag between variations in H_{mesop} and H_{PMC} is observed in most cases, as both are controlled by the T variations that, in turn, are strongly affected by tides and vertically and horizontally propagating gravity waves. For some cases in Table 1, however, the time lag varies from 0.6 to 4.4 days. We speculate that this could be partially attributed to the ice growth times. Even when the temperature is sufficiently low to allow the mesospheric ice formation, the particles initially are too small to be seen

Table 1. Linear Correlation Coefficients K_{corr} Between Mesopause Height H_{mesop} and PMC Peak Altitude H_{PMC} and Time Lag Values That Provide the Largest K_{corr}

Year, Hemisphere	Lat = 60°		Lat = 70°		Lat = 80°	
	K_{corr}	Lag (days)	K_{corr}	Lag (days)	K_{corr}	Lag (days)
2002, NH	−0.50	0	0.40	0.8	0.33	0
2003, NH	-	-	-	-	-	-
2004, NH	0.81	0	0.30	0	0.44	0.9
2005, NH	0.58	0	0.54	−0.5	0.55	3.7
2006, NH	0.46	0	0.53	0	0.78	0
2007, NH	0.8	1.5	0.64	−0.2	0.74	0
2008, NH	0.58	0	0.54	2.3	0.58	1.9
2002/2003, SH	0.66	0	0.3	1.9	-	-
2003/2004, SH	0.4	0	-	-	-	-
2004/2005, SH	-	-	-	-	0.8	1.2
2005/2006, SH	-	-	-	-	-	-
2006/2007, SH	-	-	0.8	4.4	0.7	0.6
2007/2008, SH	0.6	0	-	-	0.49	0

by OSIRIS. According to various studies, the mesospheric ice growth time from the smallest postnucleation sizes of <2 nm to optically visible sizes may vary from less than an hour to more than a day [e.g., *von Zahn and Berger*, 2003; *Mauersberger and Krankowsky*, 2003; *Rapp and Thomas*, 2006; *Zasetsky et al.*, 2009b]. Such considerable differences in the estimated ice growth times can be caused, besides the unknowns and uncertainties in the ice nucleation and growth mechanisms at mesospheric conditions, by variations in the temperature of air that surrounds growing particles. Dynamical processes may also play role in the observed time lag if ice particles in the detected PMCs have nucleated and grown to optically visible sizes at a different location [*Gadsden*, 1998; *Berger and von Zahn*, 2007] while there was no PMC particles in the considered air volume. According to *Berger and von Zahn* [2007], the horizontal transport time of PMC particles observed above 69°N at ALOMAR varies from 10 to 90 h and depends strongly on the meridional winds. We note that meridional transport effects make the correlation partially nonlocal that may explain small values of the K_{corr} for some cases listed in Table 1.

[20] Another result in Figure 1 is the reverse latitudinal dependence in mesospheric and PMC altitudes in the NH. In most cases, H_{PMC} is noticeably 0.5–0.7 km higher at 55°N–65°N than poleward of 65°N. This is observed for all seasons except 2008. H_{mesop}, however, has the opposite latitudinal dependence: it is lowest at 55°N–65°N but increases toward the pole. This can be explained by different environmental conditions and not very different temperature lapse rates at these altitudes. As midlatitude areas experience only sporadic drops of T_{mesop} below the frost point temperature, the vertical extent of the area suitable for PMC formation is likely to be smaller. At high latitudes, however, T_{mesop} drops significantly below the frost point, so the vertical size of the ice forming area is likely to be larger. This is illustrated in Figures 2 and 3 (top frames), where T_{mesop} for various latitude belts is shown. As follows from our analysis, at 75°–85°N T_{mesop} can decrease by up to 22 K from the beginning to the middle of the season and be as low as 120 K. At 55°N–65°N, the seasonal decrease in T_{mesop} is smaller, 10 K or less, and the lowest T_{mesop} is about 137 K. We have to note that such reverse latitudinal dependence has not been observed by lidars [*Lübken et al.*, 2008]. In their Figure 3, the PMC altitudes gradually decrease from 78.2°N to 69.3°N, 67.0°N, and 54.1°N. This could be due to a much lower statistics of PMC detections by OSIRIS at lower latitudes, as well as the averaging over all longitudes whereas the lidar was always stationary. A recently reported longitudinal variability in the upper mesospheric properties due to orographic gravity waves [e.g., *Chandran et al.*, 2009] may affect zonally averaged and local comparisons.

[21] OSIRIS daily mean PMC occurrence rates smoothed with a 7 day sliding window are shown on the bottom frames of Figures 2 and 3. As expected, PMC occurrence rates anticorrelate with T_{mesop}. At high latitudes of 75°–85° N/S, where T_{mesop} is typically much lower compared to that at midlatitudes, the cloud occurrence rate reaches nearly 100% from solstice and onward. At lower latitudes, PMCs are less frequent, which agrees well with higher T_{mesop}. Warmer than usual T_{mesop} in the NH in 2002 in Figure 2, discussed before by various authors [*Goldberg et al.*, 2004; *Bailey et al.*, 2005; *Petelina et al.*, 2006a, 2007], is accompanied by the late start of the season and lower cloud occurrence rates.

[22] Figure 4 shows the correlation between daily mean T_{mesop} and daily PMC occurrence rates. In Figure 4, polar and midlatitude points are mixed together assuming same PMC physics in these regions. We also found that for this correlation T_{mesop} appears to be a better characterizing parameter compared to daily mean temperature at the average PMC peak altitude T_{PMC}.

[23] The number of overlapping days for SABER and OSIRIS is 1654 and 844 for the NH and SH, respectively. The temperature data are averaged over 1 K bins, and the standard deviations are plotted for each correlation curve. The correlation of PMC occurrence rates with T_{mesop} in the NH and SH is similar. This indicates that the physics of ice particles nucleation and growth is same in both hemispheres, as expected.

[24] Both NH and SH cloud occurrence rates in Figure 4 reach a 100% plateau at $T_{mesop} \approx 125$ K. The daily PMC occurrence rates decrease to ~5% as the daily mean T_{mesop} increase to 150 K. Our result is in a good qualitative agreement with another available temperature-PMC data set from AIM [*Hervig et al.*, 2009] but differs from it quantitatively as the instruments have different sensitivity to ice particle sizes. Summarizing, T_{mesop} appears to be a proper characteristic parameter for PMC analysis, as it is related to both the minimal temperature and the vertical size of the area where ice particles can form (this will be further discussed in section 3.3.3). On the other hand, T_{PMC} is only indirectly related to the properties of ice formation area. Combined with possible offsets in PMC height/temperature assignments, this makes T_{PMC} less suitable for correlative analysis.

3.3. Comparison of "Instantaneous" Profiles

3.3.1. Coincidence Criteria

[25] As the mesospheric area is very sensitive to the energy balance processes, dynamics, and winds, the temporal and spatial variability of its physical parameters is also high. Various high-quality temperature measurements with lidars, wind measurements with radars, ground-based PMC

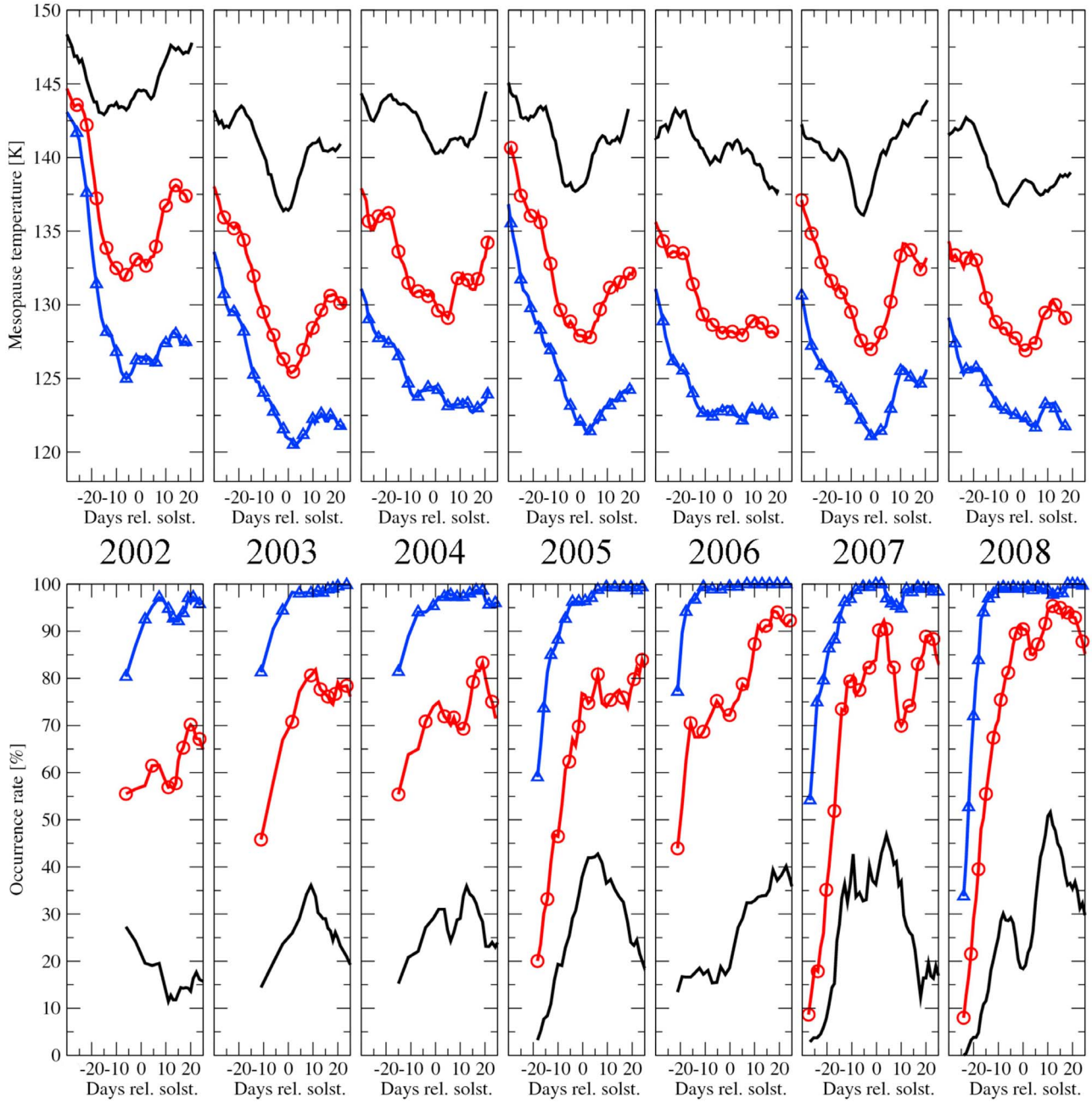

Figure 2. (top) SABER zonal mean mesopause temperatures and (bottom) OSIRIS zonal mean PMC occurrence rates in the NH. Solid curves, latitudes 55°N/S–65°N/S; curves with circles, latitudes 65°N/S–75°N/S; curves with triangles, latitudes 75°N/S–85°N/S.

photography and airglow imagery suggest that small-scale structures associated with gravity waves may vary on a time scale of minutes [e.g., *Sica et al.*, 2002; *Hoppe and Fritts*, 1995]. This implies that cloud altitudes and brightness may also vary on this time scale and imposes strict coincidence criteria between two satellite measurements. The SABER and OSIRIS data sets were searched for coincidences using an "overlapping weight" γ calculated from the following empirical formula [*Feofilov et al.*, 2009],

$$\gamma = \Delta t \times 4 + \Delta\eta \times 5 + \Delta\zeta \times 1 + 6/(90 - \theta_z),$$

where Δt is the time difference between the scans (hours), $\Delta\eta$ is the latitude difference (degrees), $\Delta\zeta$ is the longitude difference (degrees), θ_z is the solar zenith angle (degrees), and numbers 4, 5, 1, and 6 are empirically found coefficients that help to identify the "best overlap." If there were several SABER scans for a given OSIRIS measurement, we selected the one that had smaller γ value. All scans with at least one of the following conditions not satisfied: $\Delta t < 1$ h, $\Delta\eta < 4°$, $\Delta\zeta < 20°$, $\theta_z < 89°$ were excluded from the analysis.

[26] These criteria provided 1083 overlappings between SABER and OSIRIS measurements in 2002–2008. The

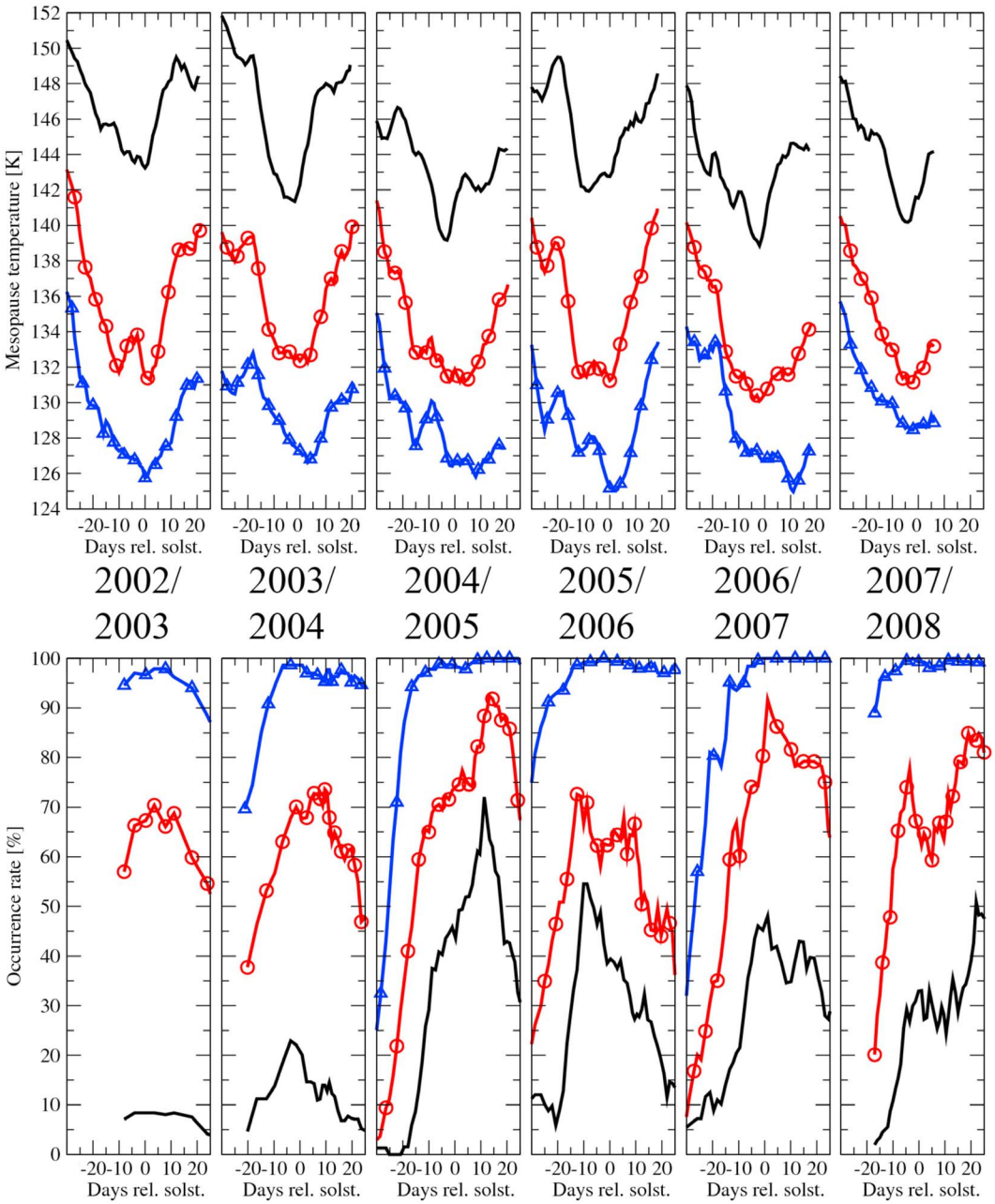

Figure 3. Same as in Figure 2, but for the SH.

average overlapping parameters with the corresponding standard deviations were $\Delta t_{aver} = 13 \pm 9$ min, $\Delta \eta_{aver} = 0.7 \pm 0.6°$, $\Delta \zeta_{aver} = 3.2 \pm 2.3°$. For each OSIRIS PMC measurement, only altitude and brightness of the cloud peak were considered. Out of those 1083 coincidences, PMCs were not observed in 561 cases, which left 522 cases for analysis.

3.3.2. Tangent Point, Near- and Far-Field Measurements, and T_{frost}

[27] OSIRIS detects PMCs using the limb-scattered sunlight and therefore measures clouds located not only at the tangent point but also in the near and/or far field of view. This may lead to an incorrect attribution of the cloud altitude: PMCs located in the near or far field of view will be assigned to lower tangent heights. A 100 km distance between the actual cloud location along the line of sight and the instrument tangent point results in ~1 km altitude error. Similarly, a 200 km distance leads to ~4 km error in cloud altitude. This uncertainty is impossible to resolve using the OSIRIS data alone. However, if such limb-measured PMCs are supplemented with pressure, temperature, and water vapor measurements from another instrument, one can rule out clouds that are outside of the physically allowed range.

[28] In this work, PMCs are selected in the following way: for each coincident OSIRIS and SABER measurement, the lowest allowed PMC altitude is set to that where the kinetic temperature T_{kin} crosses the lower frost point temperature T_{frost}. The latter is calculated for each individual coincidence

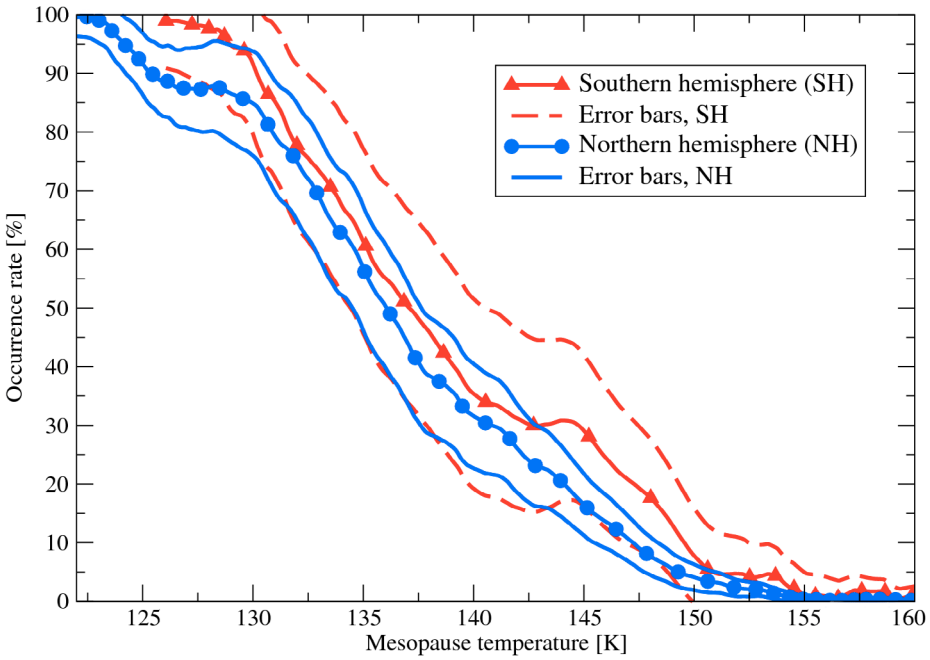

Figure 4. Correlation between SABER daily mean mesopause temperature, as well as SABER daily mean temperature at PMC peak altitude, and OSIRIS daily PMC occurrence rates in the NH and SH in 2002–2008. Solid and dashed curves without symbols indicate the standard deviations in the NH and SH, respectively.

using the SABER temperature, pressure, and water vapor VMR measurements, and the empirical formula from *Murphy and Koop* [2005]. This excludes PMCs located below the calculated lowest possible altitude. As a result of this selection, the number of "allowed" PMCs became 268 out of total 522.

[29] The above approach does not guarantee the elimination of all near- and far-field cloud detections but significantly reduces their number. As follows from our analysis, about 50% of all coincidences were below the tangent point, and almost all "allowed" PMCs were within the 81.5–86.5 km altitude range. This range agrees well with the results of various ground-based lidar measurements in both hemispheres [e.g., *Thayer et al.*, 2003; *Chu et al.*, 2006]. It is interesting that some of these "not allowed" PMCs were located at very high altitudes, up to 89 km. This could be explained by high spatial and temporal variability in the upper mesospheric characteristics. In this case instruments on different satellites may observe very different, although nearly coincident, states of the atmosphere. There were also cases when altitudes for "allowed" PMCs were higher than typical, up to 90 km, particularly in the SH. This can occur in the beginning of the season when first ice particles form near the mesopause, as well as at any time when the dynamical processes elevate the mesopause to higher altitudes, which was the case in the SH during the first half of a 2007–2008 PMC season [e.g., *Kirkwood et al.*, 2008].

[30] OSIRIS PMC data set contains all upper mesospheric observations, including non-PMC locations where a cloud would have been observed if it was there. For about 50% of all OSIRIS and SABER coincidences, no PMCs were observed even when the corresponding temperatures were low enough for ice particles to exist. Similar result was reported earlier by *Petelina et al.* [2005]. We attribute such cases to the physics of PMC growth. The growth time of mesospheric ice from subvisible to optically visible sizes varies from less than an hour to almost a day [e.g., *Zasetsky et al.*, 2009b, and references therein]. Thus even if the $T_{kin} \leq T_{frost}$ condition is satisfied for a particular location, the duration of this cold period could have been not long enough to produce ice particles of optically detectable sizes.

3.3.3. PMC Brightness Against Temperature and Water Vapor VMR

[31] Figure 5 shows the relation between PMC brightness and vertical extent of the area L_{frost} where ice particles can exist; the altitude region where the temperature is below the frost point temperature. L_{frost} area is calculated using the formulae from *Murphy and Koop* [2005], as well as pressure, temperature, and H_2O VMR values measured by SABER. Large scattering of individual points for PMC brightness in Figure 5 can be attributed to a combination of experimental uncertainties, including temperature uncertainty that is quite significant in this area: 5.4 K at 85 km for an individual profile [*Remsberg et al.*, 2008]. However, the cloud brightness averaged for each 1 km altitude bin (blue curve) shows a nearly linear increase with the increase in L_{frost}. This is in agreement with the known microphysics of mesospheric ice particles: they are very small at higher altitudes where they nucleate become larger as they grow to optically detectable sizes, sediment to lower altitudes as the growth continues, and finally evaporate when $T > T_{frost}$ [e.g., *von Savigny et al.*, 2005; *Rapp and Thomas*, 2006]. Thus, the larger the area L_{frost} is, the more time ice particles have to grow to bigger sizes and the brighter the observed PMCs are. As the amount of water vapor is very important for ice growth [e.g., *Karlsson and Rapp*, 2006],

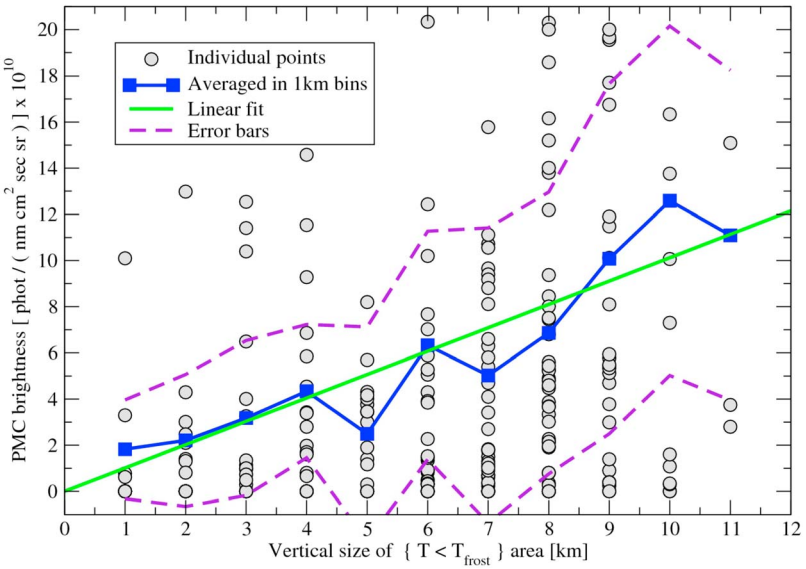

Figure 5. PMC brightness against vertical size of the frost area L_{frost}, where $T < T_{frost}$. Gray circles, individual nearly coincident measurements; curve with filled squares, the average PMC brightness for each 1 km vertical bin; solid line: linear least square fit to individual data points; dashed curves, standard deviation.

the larger vertical extent of the supersaturated altitude range may imply a larger amount of water vapor available for deposition on ice particles.

[32] Table 2 contains coefficients of linear correlation K_{corr} between PMC brightness and parameters of the surrounding region: the vertical extent of the frost area L_{frost}, the mesopause temperature T_{mesop}, the water vapor VMR "inside the cloud" H_2O_{cloud}, and the water vapor VMR below the cloud $H_2O_{undercloud}$. We define H_2O_{cloud} as the average H_2O VMR in the area $T < T_{frost}$. Likewise, $H_2O_{undercloud}$ is the average H_2O VMR within a 2 km layer below the lower $T = T_{frost}$ point. All correlations are calculated for two subsets of the 266 coincidences selected in section 3.2.2: 106 events before solstice (marked "bs") and 160 events after solstice (marked "as").

[33] As follows from Table 2, K_{corr} between PMC brightness and L_{frost} (further denoted as PMC-L_{frost}) before and after solstice are different. Higher correlation is observed after solstice, when PMCs are more frequent and brighter. As anticipated, K_{corr} between the PMC brightness and the mesopause temperature T_{mesop} (further denoted as PMC-T_{mesop}) is negative: the cloud brightness is lower when the mesopause is warmer and vice versa. The absolute value of K_{corr} for PMC-T_{mesop} after solstice is comparable to that for PMC-L_{frost}. This could provide another interpretation for the observed inverse proportionality between PMCs and temperature. As the temperature gradient below the mesopause is almost constant, L_{frost} is almost linearly inversely proportional to T_{mesop}, making these parameters well correlated.

[34] The correlations of PMC brightness with H_2O_{cloud} and $H_2O_{undercloud}$ before and after solstice differ: there is almost no correlation for PMC-H_2O_{cloud} before solstice while there is a noticeable anticorrelation of these parameters after solstice. On the other hand, the PMC-$H_2O_{undercloud}$ correlation is larger before solstice. The PMC-H_2O_{cloud} anticorrelation is expected, as well as the correlation for PMC-$H_2O_{undercloud}$. However, one could anticipate a better synchronization of these parameters as the decrease in gaseous H_2O_{cloud} related to the freeze-drying effect should cause an increase in $H_2O_{undercloud}$. If we introduce a new combined parameter (CP) as CP = $H_2O_{undercloud}/H_2O_{cloud}$, then the correlation of CP with PMCs will correspond to the correlations of its components with PMCs. This correlation reaches 0.53 for events after solstice.

[35] Figure 6 shows CP against cloud brightness for (a) individual events and (b) scatterplot with individual points, 40 point average, and a linear fit. There is an apparent CP-PMC correlation for most major peaks in CP and major peaks in PMC brightness: brighter clouds correspond to higher ratio of water vapor VMR below the cloud to water vapor VMR in the area L_{frost}. However, this correlation is not purely linear as the observed picture is not one-dimensional, local, and stationary. PMC brightness is also affected by particle growth mechanisms and mesospheric dynamics. Yet the observed correlation proves that

Table 2. Linear Correlation Coefficients K_{corr} Between PMC Brightness and L_{frost}, T_{mesop}, H_2O_{cloud}, and $H_2O_{undercloud}$[a]

Parameter	K_{corr}
L_{frost}, bs	0.17
L_{frost}, as	0.33
T_{mesop}, bs	−0.29
T_{mesop}, as	−0.38
H_2O_{cloud}, bs	0.11
H_2O_{cloud}, as	−0.44
$H_2O_{undercloud}$, bs	0.38
$H_2O_{undercloud}$, as	0.12
$H_2O_{undercloud}/H_2O_{cloud}$, bs	0.32
$H_2O_{undercloud}/H_2O_{cloud}$, as	0.53

[a]"bs" and "as" stand for "before solstice" and "after solstice," respectively.

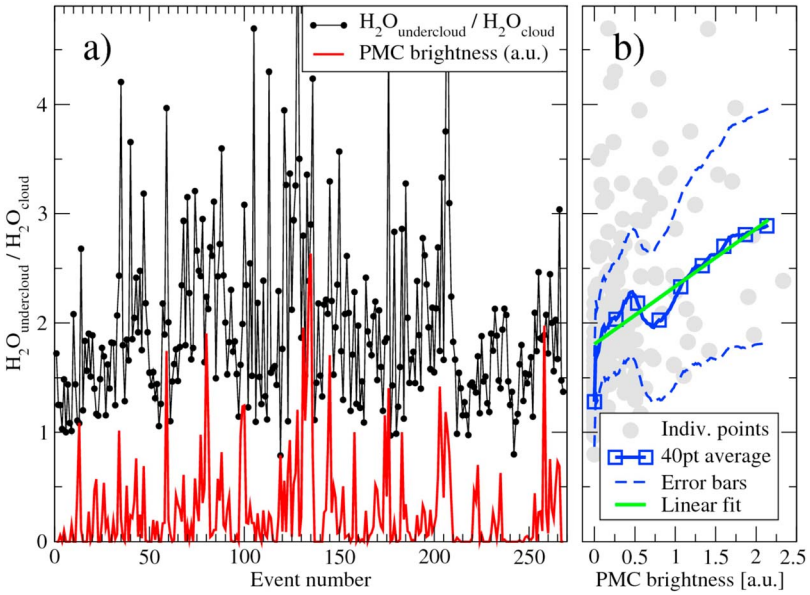

Figure 6. (a) $H_2O_{undercloud}/H_2O_{cloud}$ and PMC brightness (in arbitrary units) for 266 OSIRIS-SABER coincidences. (b) Correlation plot for the events from Figure 6a with standard deviation (dashed curves) and linear fit (solid line).

in the first approximation the lifecycle of water in the cloud area can be described as "freezing-precipitation-sublimation" scheme.

4. Summary

[36] OSIRIS and SABER satellite data sets on NH and SH PMC properties and mesospheric temperature and water vapor VMR obtained in 2002–2008, both zonal averages and close coincidences, are analyzed in this work. The daily mean PMC peak altitudes are well correlated with the daily mean mesopause altitudes in the NH, while the SH demonstrates smaller number of cases with a good correlation. The PMC peak altitudes, however, do not vary as much as the mesopause altitudes because of the restrictions on the lower cloud boundary imposed by temperature and restrictions on the upper cloud boundary due to a limited OSIRIS sensitivity to small particles. For both hemispheres, variations in PMC peak altitude generally show zero time lag with respect to variations in mesopause altitudes, although in several cases the delay time varied from 0.6 to 4.4 days. We attribute this to ice growth times and dynamics effects. Even if temperatures are favorable for the ice formation and growth, the particles initially may be too small to form optically detectable clouds. Meridional transport of the PMC particles that were formed far away from their detected location also contributes to the observed time lag in case when the considered air volume does not contain detectable PMCs.

[37] There is a reverse latitudinal dependence in the mesopause and PMC altitudes in the NH. Cloud peak altitudes at 55°N–65°N are noticeably 0.5–0.7 km higher than those poleward of 65°N for all seasons except 2008. The mesopause altitudes, however, show the opposite latitudinal dependence: they are lowest at 55°N–65°N but increase toward the pole. At high latitudes of 75°N–85°N, daily mean mesopause temperatures decrease by up to 22 K from the beginning to the middle of the PMC season and can be as low as 120 K. At 55°N–65°N, such variability in temperature is smaller, 10 K or less, and the minimum daily mean T_{mesop} does not drop below 137 K. This reversal latitudinal dependence in mesospheric and PMC altitudes is not readily seen in the SH. As the SH PMCs generally do not spread equatorward as much as the NH PMCs, such behavior in the SH is more difficult to detect. Interhemispheric differences in latitudinal dependence of mesopause temperatures and altitudes also contribute to the observed effect. As follows from our analysis, at high latitudes a generally larger difference between NH and SH mesopause heights is observed, while at low latitudes a generally larger difference in NH and SH mesopause temperatures is seen. Variations in H_{mesop} and H_{PMC} appear to be correlated with correlation coefficient reaching 0.7–0.8 for some seasons. In general, H_{mesop} and H_{PMC} are better correlated in the NH where $K_{corr} > 0.5$ for more than half of the cases.

[38] PMC occurrence rates correlate with mesopause temperatures similarly in the NH and SH. This indicates that the physics of ice particles formation and growth is same in both hemispheres, as expected. The interhemispheric variability in PMC-T_{PMC} curves is stronger than the interhemispheric variability in PMC-T_{mesop} curves. As ice particles start to nucleate and grow at altitudes higher than the cloud peak altitudes, T_{PMC} is only indirectly linked to the properties of ice formation area. On the other hand, T_{mesop} appears to be a better characteristic parameter for the mesospheric ice properties as it is related to both the minimal temperature and the vertical size of the area where ice particles form.

[39] For about 50% of all coincidences between two instruments, no PMCs were observed by OSIRIS even when their existence was "allowed" according to the SABER frost point temperature analysis. As the ice growth time varies

greatly, even for $T_{kin} \leq T_{frost}$ the duration of such cold period could have been not long enough to produce ice particles of optically detectable sizes. For all OSIRIS and SABER coincidences with PMCs, about 50% of clouds were found to be outside the "allowed" region. While most of such "not allowed" clouds were located below the tangent point, some were observed at very high altitudes near 89 km, possibly because two instruments have seen very different atmospheric states. The majority of the "allowed" PMCs were located at altitudes of 81.5–86.5 km and few clouds were found at high altitudes near 90 km.

[40] The correlation between OSIRIS PMC brightness and the vertical extent of the frost area, mesopause temperature, water vapor VMR in and below the cloud is always higher for observations made after solstice. The highest correlation, 0.53, is observed between the cloud brightness and the water content in and below the cloud for events after solstice. This is in agreement with our current understanding of the region's physics: freeze-drying is observed in the cloud formation area, the hydration effects can be seen below the cloud, and the PMC brightness is proportional to the size of the area where $T < T_{frost}$.

[41] **Acknowledgments.** This research was partially supported under NASA grant NNX08AG41G. The authors are grateful to the SABER science, data processing, and flight operations for their ongoing support of this work. Odin is a Swedish-led satellite project funded jointly by Sweden (SNSB), Canada (CSA), France (CNES), and Finland (Tekes). Odin is presently a third party mission for the European Space Agency (ESA) and the OSIRIS data are provided by ESA.

References

Bailey, S. M., A. W. Merkel, G. E. Thomas, and D. W. Rusch (2005), Observations of polar mesospheric clouds by the Student Nitric Oxide Explorer, *J. Geophys. Res.*, *110*, D13203, doi:10.1029/2004JD005422.

Berger, U., and U. von Zahn (2007), Three-dimensional modeling of the trajectories of visible noctilucent cloud particles: An indication of particle nucleation well below the mesopause, *J. Geophys. Res.*, *112*, D16204, doi:10.1029/2006JD008106.

Bernath, P. F., et al. (2005), Atmospheric Chemistry Experiment (ACE): Mission overview, *Geophys. Res. Lett.*, *32*, L15S01, doi:10.1029/2005GL022386.

Chandran, A., D. W. Rusch, S. E. Palo, G. E. Thomas, and M. J. Taylor (2009), Gravity wave observations in the summer time polar mesosphere from the Cloud Imaging and Particle Size (CIPS) experiment on the AIM spacecraft, *J. Atm. Solar-Terr. Phys.*, *71*, 392–400.

Chu, X. Z., P. J. Espy, G. J. Nott, J. C. Diettrich, and C. S. Gardner (2006), Polar mesospheric clouds observed by an iron Boltzmann lidar at Rothera (67.5°S, 68.0°W), Antarctica from 2002 to 2005: Properties and implications, *J. Geophys. Res.*, *111*, D20213, doi:10.1029/2006JD007086.

DeLand, M. T., E. P. Shettle, G. E. Thomas, and J. J. Olivero (2006), A quarter-century of satellite polar mesospheric cloud observations, *J. Atm. Solar-Terr. Phys.*, *68*, 9–29, doi:10.1016/j.jastp.2005.08.003.

Edwards, D. P., G. Zaragoza, M. Riese, and M. López-Puertas (2000), Evidence of H_2O nonlocal thermodynamic equilibrium emission near 6.4 μm as measured by cryogenic infrared spectrometers and telescopes for the atmosphere (CRISTA 1), *J. Geophys. Res.*, *105*(23), 29,003–29,021, doi:10.1029/2000JD900350.

Eremenko, M. N., S. V. Petelina, A. Y. Zasetsky, B. Karlsson, C. P. Rinsland, E. J. Llewellyn, and J. J. Sloan (2005), Shape and composition of PMC particles derived from satellite remote sensing measurements, *Geophys. Res. Lett.*, *32*, L16S06, doi:10.1029/2005GL023013.

Feofilov, A. G., et al. (2009), Daytime SABER/TIMED observations of water vapor in the mesosphere: retrieval approach and first results, *Atmos. Chem. Phys.*, *9*, 8139–8158.

Fiedler, J., G. Baumgarten, and G. von Cossart (2005), Mean diurnal variations of noctilucent clouds during 7 years of lidar observations at ALOMAR, *Ann. Geophys.*, *23*, 1175–1181.

Gadsden, M. (1998), Noctilucent clouds seen at 60N: Origin and development, *J. Atmos. Sol. Terr. Phys.*, *60*, 1763–1772.

Goldberg, R. A., et al. (2004), The MaCWAVE/MIDAS rocket and ground-based measurements of polar summer dynamics: Overview and mean state structure, *Geophys. Res. Lett.*, *31*, L24S02, doi:10.1029/2004GL019411.

Gumbel, J., J. Stegman, D. P. Murtagh, and G. Witt (2001), Scattering phase function and particle sizes in Noctilucent clouds, *Geophys. Res. Lett.*, *28*(8), 1415–1418, doi:10.1029/2000GL012414.

Gusev, O. A., and A. A. Kutepov (2003), Non-LTE gas in planetary atmospheres, in *Stellar Atmosphere Modeling*, edited by I. Hubeny, D. Mihalas, and K. Werner, *ASP Conference Series*, 288, 318–330.

Hervig, M., R. Thompson, M. McHugh, L. Gordley, J. Russell III, and M. Summers (2001), First confirmation that water ice is the primary component of polar mesospheric clouds, *Geophys. Res. Lett.*, *28*(6), 971–974, doi:10.1029/2000GL012104.

Hervig, M. E., L. L. Gordley, J. M. Russell III, and S. M. Bailey (2009), SOFIE PMC observations during the northern summer of 2007, *J. Atmos. Solar-Terr. Phys.*, *71*, 331–339, doi:10.1016/j.jastp.2008.08.010.

Hoppe, U.-P., and D. C. Fritts (1995), High-resolution measurements of vertical velocity with the European incoherent scatter VHF radar: 1. Motion field characteristics and measurement bias, *J. Geophys. Res.*, *100*(D8), 16,813–16,825, doi:10.1029/95JD01466.

Karlsson, B., and M. Rapp (2006), Latitudinal dependence of noctilucent cloud growth, *Geophys. Res. Lett.*, *33*, L11812, doi:10.1029/2006GL025805.

Kirkwood, S., et al. (2008), A new height for the summer mesopause: Antarctica, December 2007, *Geophys. Res. Lett.*, *35*, L23810, doi:10.1029/2008GL035915.

Kutepov, A. A., O. A. Gusev, and V. P. Ogibalov (1998), Solution of the non-LTE problem for molecular gas in planetary atmospheres: Superiority of accelerated lambda iteration, *J. Quant. Spectrosc. Rad. Transfer*, *60*, 199–220.

Kutepov, A. A., A. G. Feofilov, B. T. Marshall, L. L. Gordley, W. D. Pesnell, R. A. Goldberg, and J. M. Russell III (2006), SABER temperature observations in the summer polar mesosphere and lower thermosphere: importance of accounting for the CO_2 ν_2-quanta V–V exchange, *Geophys. Res. Lett.*, *33*, L21809, doi:10.1029/2006GL026591.

Llewellyn, E. J., et al. (2004), The OSIRIS instrument on the Odin spacecraft, *Can. J. Phys.*, *82*, 411–422, doi:10.1139/P04-005.

López-Puertas, M., and F. W. Taylor (2001), *Non-LTE Radiative Transfer in the Atmosphere*, 504 pp., World Scientific Publishing Co., River Edge, N.J.

López-Puertas, M., G. Zaragoza, B. J. Kerridge, and F. W. Taylor (1995), Non-local thermodynamic equilibrium model for H_2O 6.3 and 2.7 μm bands in the middle atmosphere, *J. Geophys. Res.*, *100*(D5), 9131–9147, doi:10.1029/95JD00383.

Lübken, F.-J. (1999), Thermal structure of the Arctic summer mesosphere, *J. Geophys. Res.*, *104*(D8), 9135–9149, doi:10.1029/1999JD900076.

Lübken, F.-J., M. Rapp, and I. Strelnikova (2007), The sensitivity of mesospheric ice layers to atmospheric background temperatures and water vapor, *Adv. Space Res.*, *40*, 794–801.

Lübken, F.-J., G. Baumgarten, J. Fiedler, M. Gerding, J. Höffner, and U. Berger (2008), Seasonal and latitudinal variation of noctilucent cloud altitudes, *Geophys. Res. Lett.*, *35*, L06801, doi:10.1029/2007GL032281.

Manuilova, R. O., V. A. Yankovsky, A. O. Semenov, O. A. Gusev, A. A. Kutepov, O. N. Sulakshina, and Yu. G. Borkov, (2001), Non-equilibrium emission of the middle atmosphere in the IR ro-vibrational water vapor bands, *Atmos. Ocean. Opt.*, *14*, 864–867.

Mauersberger, K., and D. Krankowsky (2003), Vapor pressure above ice at temperatures below 170 K, *Geophys. Res. Lett.*, *30*(3), 1121, doi:10.1029/2002GL016183.

Murphy, D. M., and T. Koop (2005), Review of the vapour pressures of ice and supercooled water for atmospheric applications, *Quart. J. Royal Meterol. Soc.*, *131*, 1539–1565.

Murray, B. J., and E. J. Jensen (2009), Homogeneous nucleation of amorphous solid water particles in the upper mesosphere, *J. Atmos. Solar-Terr. Phys.*, *72*, 51–61, doi:10.1016/j.jastp.2009.10.007.

Murtagh, D. P., et al. (2002), An Overview of the Odin Atmospheric Mission, *Can. J. Phys.*, *80*(4), 309–319.

Petelina, S. V., D. A. Degenstein, E. J. Llewellyn, N. D. Lloyd, C. J. Mertens, M. G. Mlynczak, and J. M. Russell III (2005), Thermal conditions for PMC existence derived from Odin/OSIRIS and TIMED/SABER data, *Geophys. Res. Lett.*, *32*, L17813, doi:10.1029/2005GL023099.

Petelina, S. V., E. J. Llewellyn, D. A. Degenstein, and N. D. Lloyd (2006a), Odin/OSIRIS limb observations of Polar Mesospheric Clouds in 2001–2003, *J. Atmos. Solar-Terr. Phys.*, *68*, 42–55, doi:10.1016/j.jastp.2005.08.004.

Petelina, S. V., D. A. Degenstein, E. J. Llewellyn, and N. D. Lloyd (2006b), Correlation of PMC relative brightness and altitudes observed

by Odin/OSIRIS in the Northern Hemisphere in 2002–2003, *J. Atmos. Solar-Terr. Phys.*, *68*, 56–64, doi:10.1016/j.jastp.2005.08.005.

Petelina, S. V., E. J. Llewellyn, and D. A. Degenstein (2007), Properties of polar mesospheric clouds measured by Odin/OSIRIS in the Northern Hemisphere in 2002–2005, *Can. J. Phys.*, *85*, 1143–1158.

Rapp, M., and G. E. Thomas (2006), Modeling the microphysics of mesospheric ice particles: Assessment of current capabilities and basic sensitivities, *J. Atmos. Solar-Terr. Phys.*, *68*, 715–744.

Remsberg, E. E., et al. (2008), Assessment of the quality of the Version 1.07 temperature-versus-pressure profiles of the middle atmosphere from TIMED/SABER, *J. Geophys. Res.*, *113*, D17101, doi:10.1029/2008JD010013.

Robert, C. E., C. von Savigny, J. P. Burrows, and G. Baumgarten (2009), Climatology of noctilucent cloud radii and occurrence frequency using SCIAMACHY, *J. Atmos. Solar-Terr. Phys.*, *71*, 408–423, doi:10.1016/j.jastp.2008.10.015.

Rybicki, G. B., and D. G. Hummer (1991), An accelerated lambda iteration method for multilevel radiative transfer: I. Non-overlapping lines with background continuum, *Astron. Astrophys.*, *245*, 171–181.

Shettle, E. P., M. T. DeLand, G. E. Thomas, and J. J. Olivero (2009), Long term variations in the frequency of polar mesospheric clouds in the Northern Hemisphere from SBUV, *Geophys. Res. Lett.*, *36*, L02803, doi:10.1029/2008GL036048.

Sica, R. J., T. Thayaparan, P. S. Argall, A. T. Russell, and W. K. Hocking (2002), Modulation of upper mesospheric temperature inversions due to tidal-gravity wave interactions, *J. Atmos. Solar-Terr. Phys.*, *64*(8–11), 915–922.

Stevens, M., C. Englert, M. Hervig, S. V. Petelina, W. Singer, and K. Nielsen (2009), The diurnal variation of noctilucent clouds frequency near 55N observed by SHIMMER, *J. Atmos. Solar-Terr. Phys.*, *71*, 401–408.

Thayer, J. P., M. Rapp, A. J. Gerrard, E. Gudmundsson, and T. J. Kane (2003), Gravity-wave influences on Arctic mesospheric clouds as determined by a Rayleigh lidar at Sondrestrom, Greenland, *J. Geophys. Res.*, *108*(D8), 8449, doi:10.1029/2002JD002363.

Thomas, G. E. (1991), Mesospheric clouds and the physics of the mesopause region, *Rev. Geophys.*, *29*(4), 553–575, doi:10.1029/91RG01604.

Thomas, G. E. (2003), Are noctilucent clouds harbingers of global change in the middle atmosphere?, *Adv. Space Res.*, *32*(9), 1737–1746.

von Savigny, C., et al. (2005), Vertical variation of NLC particle sizes retrieved from Odin/OSIRIS limb scattering observations, *Geophys. Res. Lett.*, *32*, L07806, doi:10.1029/2004GL021982.

von Zahn, U., and U. Berger (2003), Persistent ice cloud in the midsummer upper mesosphere at high latitudes: Three-dimensional modeling and cloud interactions with ambient water vapor, *J. Geophys. Res.*, *108*(D8), 8451, doi:10.1029/2002JD002409.

Witt, G. (1969), The nature of noctilucent clouds, *Space Res. IX*, 157–169.

Yee, J.-H., G. E. Cameron, and D. Y. Kusnierkiewicz (1999), Overview of TIMED, *SPIE*, *3756*, 244–254.

Zaragoza, G., M. López-Puertas, A. Lambert, J. J. Remedios, and F. W. Taylor (1998), Non-local thermodynamic equilibrium in H_2O 6.9 μm emission as measured by the improved stratospheric and mesospheric sounder, *J. Geophys. Res.*, *103*(D23), 31,293–31,308, doi:10.1029/98JD02833.

Zasetsky, A. Y., S. V. Petelina, and I. M. Svishchev (2009a), Thermodynamics of homogeneous nucleation of ice particles in the polar summer mesosphere, *Atmos. Chem. Phys.*, *9*, 965–971.

Zasetsky, A. Y., S. V. Petelina, R. Remorov, C. D. Boone, P. F. Bernath, and E. J. Llewellyn (2009b), Ice particle growth in the polar summer mesosphere: formation time and equilibrium size, *Geophys. Res. Lett.*, *36*, L15803, doi:10.1029/2009GL038727.

A. G. Feofilov, The Catholic University of America, Washington, DC 20064, USA. (artem-feofilov@cua-nasa-gsfc.info)

S. V. Petelina, La Trobe University, Melbourne, Victoria 3086, Australia.